

See discussions, stats, and author profiles for this publication at: <https://www.researchgate.net/publication/278724461>

A Gold@Polydopamine Core–Shell Nanoprobe for Long-Term Intracellular Detection of MicroRNAs in Differentiating Stem Cells

ARTICLE in JOURNAL OF THE AMERICAN CHEMICAL SOCIETY · JUNE 2015

Impact Factor: 12.11 · DOI: 10.1021/jacs.5b01457

CITATION

1

READS

48

9 AUTHORS, INCLUDING:



Kc Wei

The Chinese University of Hong Kong

7 PUBLICATIONS 105 CITATIONS

[SEE PROFILE](#)



Xu Yang

The Chinese University of Hong Kong

2 PUBLICATIONS 1 CITATION

[SEE PROFILE](#)



Meiling Zhu

Independent Researcher

9 PUBLICATIONS 100 CITATIONS

[SEE PROFILE](#)



Chung Hang Jonathan Choi

The Chinese University of Hong Kong

20 PUBLICATIONS 1,826 CITATIONS

[SEE PROFILE](#)

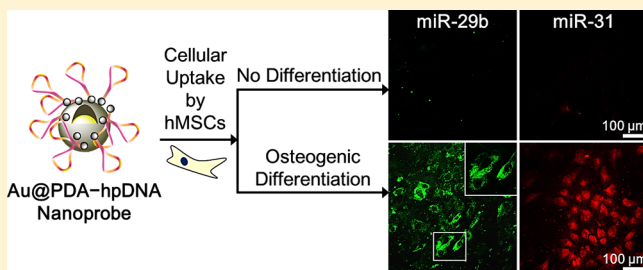
A Gold@Polydopamine Core–Shell Nanoprobe for Long-Term Intracellular Detection of MicroRNAs in Differentiating Stem Cells

Chun Kit K. Choi,[†] Jinming Li,^{†,||} Kongchang Wei,^{†,||} Yang J. Xu,[†] Lok Wai C. Ho,[‡] Meiling Zhu,[†] Kenneth K. W. To,[§] Chung Hang J. Choi,^{*,†,||} and Liming Bian^{*,†,||}

[†]Department of Mechanical and Automation Engineering (Biomedical Engineering), [‡]Department of Electronic Engineering (Biomedical Engineering), [§]School of Pharmacy, ^{||}Shun Hing Institute of Advanced Engineering, The Chinese University of Hong Kong, Shatin, New Territories, Hong Kong, China

Supporting Information

ABSTRACT: The capability of monitoring the differentiation process in living stem cells is crucial to the understanding of stem cell biology and the practical application of stem-cell-based therapies, yet conventional methods for the analysis of biomarkers related to differentiation require a large number of cells as well as cell lysis. Such requirements lead to the unavoidable loss of cell sources and preclude real-time monitoring of cellular events. In this work, we report the detection of microRNAs (miRNAs) in living human mesenchymal stem cells (hMSCs) by using polydopamine-coated gold nanoparticles (Au@PDA NPs). The PDA shell facilitates the immobilization of fluorescently labeled hairpin DNA strands (hpDNAs) that can recognize specific miRNA targets. The gold core and PDA shell quench the fluorescence of the immobilized hpDNAs, and subsequent binding of the hpDNAs to the target miRNAs leads to their dissociation from Au@PDA NPs and the recovery of fluorescence signals. Remarkably, these Au@PDA–hpDNA nanoprobes can naturally enter stem cells, which are known for their poor transfection efficiency, without the aid of transfection agents. Upon cellular uptake of these nanoprobes, we observe intense and time-dependent fluorescence responses from two important osteogenic marker miRNAs, namely, miR-29b and miR-31, only in hMSCs undergoing osteogenic differentiation and living primary osteoblasts but not in undifferentiated hMSCs and 3T3 fibroblasts. Strikingly, our nanoprobes can afford long-term tracking of miRNAs (5 days) in the differentiating hMSCs without the need of continuously replenishing cell culture medium with fresh nanoprobes. Our results demonstrate the capability of our Au@PDA–hpDNA nanoprobes for monitoring the differentiation status of hMSCs (i.e., differentiating versus undifferentiated) via the detection of specific miRNAs in living stem cells. Our nanoprobes show great promise in the investigation of the long-term dynamics of stem cell differentiation, identification and isolation of specific cell types, and high-throughput drug screening.



INTRODUCTION

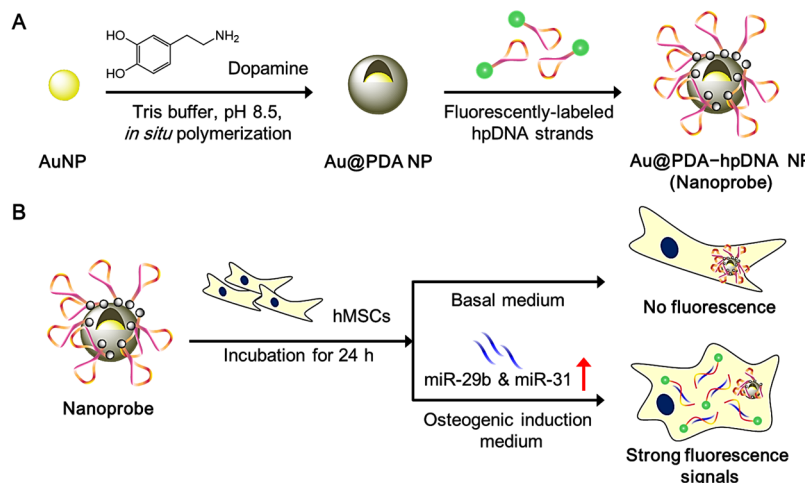
Human mesenchymal stem cells (hMSCs) serve as a very promising cell source for tissue engineering and regenerative medicine, owing to their ease of isolation and multipotency to differentiate to various lineages including adipocytes, osteoblasts, and chondrocytes.¹ Determination of the differentiation status of hMSCs (e.g., differentiating versus undifferentiated) is critical to the application of hMSCs in stem-cell-based therapies.^{2,3} To achieve this, end-point methods such as qualitative reverse transcription-polymerase chain reaction (qRT-PCR) and Western blot are conventionally utilized to confirm the expression of certain differentiation-relevant marker genes⁴ or proteins.⁵ Our in-house qRT-PCR results of two early osteogenic marker genes, namely, *RUNX2* and *ALP*, indeed show differential expression between the differentiating hMSCs and undifferentiated hMSCs upon 3 d of osteogenic induction (Figure S1). Although these analytical methods are reliable, a large number of cell samples and lysis of the cells are required for the analysis, thus leading to the

unavoidable loss of cell sources. Immunofluorescence and chemical staining are two other common methods to examine the differentiation status of fixed stem cells. However, they are not sensitive enough to monitor the early differentiation stage of stem cells (as evidenced by our in-house staining data shown in Figure S2) and also preclude real-time monitoring of intracellular activities. Newer techniques including fluorescence-activated cell sorting^{6,7} (FACS) and surface-enhanced Raman spectroscopy⁸ (SERS) offer a nondestructive alternative to sort or distinguish between differentiated and undifferentiated stem cells via examination of the changes in membranous features in living stem cells. Nevertheless, these techniques generally require expensive staining reagents or specialized instruments. They are also not suitable for detecting intracellular biomarkers. In this regard, developing a facile and noninvasive way either to monitor the differentiation process or

Received: February 9, 2015

Published: May 21, 2015

Scheme 1. (A) Preparation of the Polydopamine-Coated Gold Nanoparticles (Au@PDA NPs) and Hairpin-DNA-Based (hpDNA) Nanoprobes; (B) Intracellular Detection of miRNAs in Living Human Mesenchymal Stem Cells (hMSCs)



to distinguish the differentiation status of living stem cells is highly desirable.

NanoFlare, a polyvalent oligonucleotide functionalized nanoconstruct, has been applied for detecting intracellular messenger RNA (mRNA) levels in live cells either in culture^{9,10} or from human blood.¹¹ Because of their ability to naturally enter cells¹² and stability toward enzymatic degradation,¹³ such spherical nucleic acid (SNA) conjugates¹⁴ outperform conventional probes such as molecular beacons (MBs), which are less resistant to nucleases⁹ and often require transfection for cellular internalization.¹⁵ Despite the impressive properties of the NanoFlare, detection of cellular components in cell types with low transfection efficiency such as stem cells¹⁶ has not been reported using the system. Furthermore, as SNA has been found to be disassembled 16 h after cellular entry,¹⁷ it remains unclear whether the NanoFlare (basically a SNA nanoconstruct) can allow for long-term tracking of intracellular targets in living cells (beyond 24 h) upon a single administration.

MicroRNAs (miRNAs) are single-stranded noncoding RNAs with a typical short length of 21–23 nucleotides.¹⁸ They play an important role in controlling the expression of target proteins either via the repression of mRNAs or the inhibition of mRNA translation in a sequence-specific manner, thereby providing an additional level of gene regulation.^{19,20} In particular to stem cell studies, miRNAs have newly emerged as a mediator of various stem cell behaviors, including differentiation.^{21–24} miR-29b²⁵ and miR-31²⁶ are two distinct miRNA markers for the osteogenesis of hMSCs. Profiling studies^{18,21,27} show that these specific miRNAs are significantly up-regulated in stem cells following the osteogenic induction. The dynamic nature of these specific miRNA expression profiles mediated by osteogenic differentiation indicates that miRNAs may function as viable biomarkers for monitoring the differentiation progress of stem cells. Although much effort has been devoted to tracking intracellular mRNAs,^{9–11,28} only a few attempts have been reported to detect cancer-related miRNAs in cancerous cell lines.^{29,30} To the best of our knowledge, no prior study has demonstrated a long-term monitoring (beyond 24 h) of miRNA levels in living stem cells.

In this study, we report a novel hairpin-DNA-based nanoprobe for detecting specific miRNAs in living hMSCs. This nanoprobe possesses a core–shell structure formed by

depositing a layer of polydopamine (PDA) on the surface of a gold nanoparticle (AuNP) core via *in situ* polymerization under alkaline conditions. Such gold-PDA core–shell nanoparticles (Au@PDA NPs) are amenable to subsequent immobilization of fluorescently labeled hairpin DNA strands (hpDNAs) onto the PDA shell simply by π – π interactions (Scheme 1A). Unlike the existing intracellular detection platforms such as MBs, the resultant Au@PDA–hpDNA NPs (termed “nanoprobes”) can naturally enter stem cells without the need of transfection. And different from the NanoFlare, fabrication of our nanoprobes requires only one single type of DNA sequence that can recognize the target miRNA. Because of the close proximity between hpDNAs and the AuNP core (<5 nm)³¹ and compounded by the intrinsic quenching property of the PDA shell,³² the immobilized hpDNAs on the nanoprobes do not fluoresce appreciably. The presence of two quenching entities (i.e., AuNP core and PDA shell) makes our nanoprobes unique from the existing nanoparticle-based detection probes that typically possess only a single quenching entity such as the AuNP core of the NanoFlare. In the presence of miRNA targets with a sequence complementary to the recognition region of the immobilized hpDNAs, we show in buffer that the specific binding between the hpDNAs and the target miRNAs triggers the dissociation of hpDNAs from Au@PDA NPs, and thereafter generates detectable fluorescent signals. Using these nanoprobes, we demonstrate the specific and long-term detection of two important osteogenic marker miRNAs, namely, miR-29b and miR-31, in living hMSCs undergoing osteogenic differentiation as well as living primary osteoblasts (Scheme 1B).

RESULTS AND DISCUSSION

Preparation and Characterization of Au@PDA NPs.

We first prepare citrate-capped AuNPs of 42.3 ± 2.7 nm in diameter as the core by using a previously reported seed-mediated growth method.³³ We determine the molar concentration of the as-prepared AuNP stock solution as ~ 0.1 nM by using UV-vis spectroscopy. In addition, inductively coupled plasma optical emission spectrometry (ICP-OES) shows that the atomic Au concentration of the prepared AuNP stock is $40 \mu\text{g/mL}$. Caution is taken to maintain the original concentration of the AuNP stock during the subsequent coating process and in all of the following

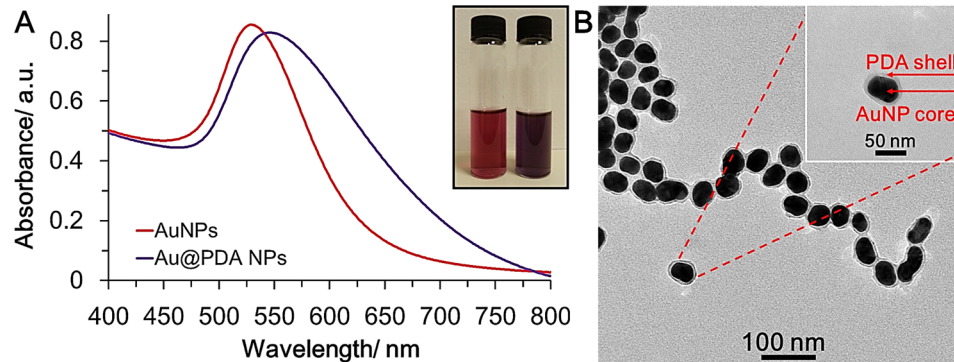


Figure 1. Characterization of Au@PDA NPs. (A) UV-vis spectra of aqueous solutions of citrate-capped AuNPs and Au@PDA NPs. Inset: Photographs of AuNPs (left) and Au@PDA NPs (right) show the color change after the coating of AuNPs with a thin PDA shell. (B) Representative TEM images of Au@PDA NPs. Inset: Magnified image of a single Au@PDA NP showing clearly its core–shell structure.

Table 1. Physiochemical Properties of AuNPs and Au@PDA NPs

sample	core size [nm] ^a	core size [nm] ^a	shell thickness [nm] ^a	physical size [nm] ^a	hydrodynamic size [nm] (PDI) ^b	zeta potential [mV] ^b
AuNPs	N.A. ^c	N.A. ^c	N.A. ^c	42.3 ± 2.7	44.6 ± 0.6 (0.25)	-31.9 ± 2.1
Au@PDA NPs	43.9 ± 3.4	43.9 ± 3.4	4.6 ± 0.3	54.5 ± 4.6	56.1 ± 1.6 (0.19)	-39.0 ± 1.5

^aThe values are obtained from the analysis of over 100 particles in multiple TEM images by ImageJ. ^bMeasured by Zeta Plus zeta potential analyzer. Results are given in mean ± SD (PDI = polydispersity index) of 10 measurements. ^cMeasurement is not applicable to the sample.

experiments. Next, we coat the AuNPs with a uniform and thin PDA shell (4.6 ± 0.3 nm) via *in situ* polymerization of dopamine, during which AuNPs are ultrasonically dispersed in a solution of dopamine buffered at pH 8.5 for 1 h.^{34,35} A very low concentration of dopamine solution, i.e., 0.05 mg/mL, is used in this study to minimize the self-polymerization of dopamine and to tune the thickness of the PDA shell. As revealed by the UV-vis absorption spectra, coating PDA on the surface of AuNPs leads to a slight red-shift of the maximum peak from 530 to 550 nm and an increase in near-infrared (NIR) absorbance (Figure 1A). The core–shell structure of Au@PDA NPs is clearly visible under transmission electron microscopy (TEM) (Figure 1B). Typical TEM images show that Au@PDA NPs possess a physical size of 54.5 ± 4.6 nm (Table 1). Dynamic light scattering (DLS) measurements (Figure S3) reveal a hydrodynamic diameter of 56.1 ± 1.6 nm for the same batch of Au@PDA NPs (Table 1). Both the TEM and DLS data collectively indicate that the Au@PDA NPs fall within a size range that favors cellular uptake by mammalian cells.^{36,37} It is worth noting that the shell thickness can be easily tuned to the desired range by simply changing the dopamine concentration (Figure S4). Table 1 summarizes the physicochemical properties of AuNPs and Au@PDA NPs. A comparison between the Fourier transform infrared (FT-IR) spectra of AuNPs and Au@PDA NPs further confirms the presence of the PDA shell on the surface of AuNPs (Figure S5). Newly emerged absorption bands at 3410 cm^{-1} (stretching vibration of phenolic O–H and N–H), 1605 cm^{-1} (stretching vibration of aromatic ring and bending vibration of N–H), 1510 cm^{-1} (shearing vibration of N–H), and 1295 cm^{-1} (stretching vibration of phenolic C–O) all indicate successful coating of PDA on the AuNPs.³⁸ Afterward, we test the colloidal stability of the Au@PDA NPs in water, PBS, and basal medium for hMSCs. UV-vis spectroscopy shows that the Au@PDA NPs are stable in those solutions for at least 24 h upon incubation at 37°C without obvious aggregation (Figure S6B). Furthermore, the PDA shell does not cause significant cytotoxicity,³⁹ as proven by our cell viability data collected

from hMSCs incubated with different concentrations of nanoparticles for 24 h (Figure S7).

Preparation and Characterization of Au@PDA–hpDNA Nanoparticles. We anticipate that the PDA shell will serve two important design purposes that support the detection of miRNAs inside stem cells. Its abundant catechol and amino groups allow for the facile and direct immobilization of DNA strands via π – π interactions and hydrogen bonding.⁴⁰ Such interactions will be weakened upon the specific binding to the complementary target miRNAs, thus resulting in the release of the immobilized DNA probes.^{41,42} Together with the AuNP core, the PDA shell also assists in quenching the emission of the fluorescently labeled hairpin DNA (hpDNA) recognition strands to be deposited on its surface,³² thereby resulting in a compounded quenching effect. For our initial studies, fluorescein isothiocyanate (FITC)-labeled hpDNA strands that specifically recognize miR-29b (sequence information listed in Table S1, denoted hpDNA-29b) are loaded onto the surface of Au@PDA NPs by gentle mixing for 1 h to form Au@PDA–hpDNA NPs (or “nanoprobes”) against miR-29b. We then compare the fluorescence of free FITC-labeled hpDNAs with that of nanoprobes immobilized with FITC-hpDNAs. Emission spectra show that the FITC fluorescence signals of 250 nM of FITC-hpDNAs (λ_{\max} located at 520 nm) are almost entirely quenched by the Au@PDA NPs (Figure 2A). These data confirm the successful adsorption of the FITC-labeled hpDNA strands onto the surface of Au@PDA NPs and highlight the excellent fluorescence quenching power of the Au@PDA NPs. To demonstrate the versatility of our Au@PDA NPs, we repeat the above quenching experiment by loading cyanine 3 (Cy3)-labeled hpDNAs that specifically target miR-31 (sequence information listed in Table S1, denoted hpDNA-31), onto the surface of Au@PDA NPs. Again, we observe effective quenching of the Cy3 fluorescence (λ_{\max} located at 570 nm) after 1 h of incubation (Figure 2A). Taking both the FITC and Cy3 quenching data together, we show that the quenching is independent of the fluorescent dye attached and the sequence of the hpDNA recognition strands. The robust

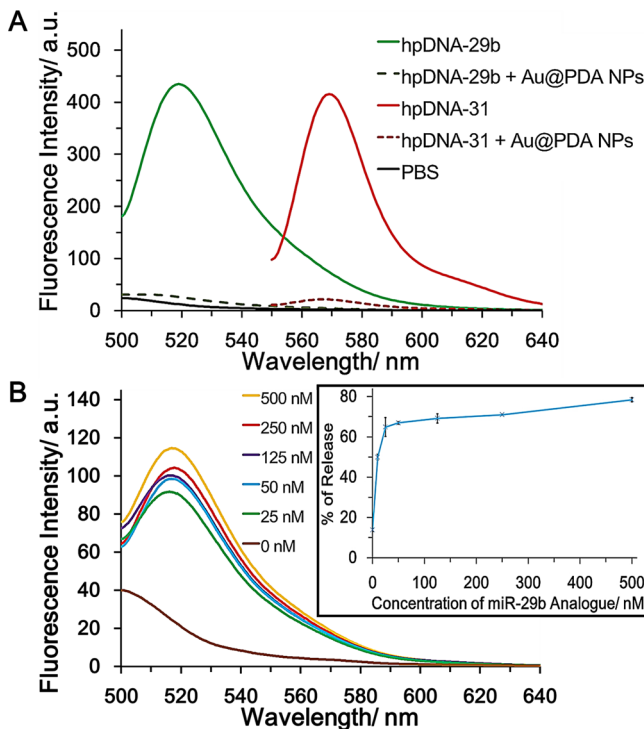


Figure 2. (A) Fluorescence emission spectra of 250 nM of fluorescently labeled hpDNA recognition strands before and after immobilization onto the surface of Au@PDA NPs. (B) Release profile of the nanoprobes for miR-29b detection in buffer. Inset: Plot of percentage of release versus concentration of DNA analogue of target miR-29b. Data obtained from 3 independent measurements are presented as mean \pm SD. FITC: Ex: 480 nm; Em: 520 nm. Cy3: Ex: 520 nm; Em: 570 nm.

quenching ability of the Au@PDA NPs may afford a high signal-to-noise ratio in the subsequent intracellular detection of miRNAs.

After characterizing the typical physiochemical properties of the nanoprobes (Table S2), we next assess the ability of the nanoprobes to release the immobilized and quenched fluorescent hpDNA strands in the presence of miRNA targets. To achieve this, we add the DNA analogue of the target miR-29b (sequence information listed in Table S1) to a buffer that contains nanoprobes against miR-29b, and subsequently observe any recovery of fluorescence signals due to the specific release of immobilized hpDNAs. 100 nM of the hpDNA recognition strands against miR-29b are first immobilized onto Au@PDA NPs as aforementioned. Upon 2 h of incubation with the DNA analogue of the target miR-29b at a concentration ranging from 25 to 500 nM, the FITC emission signals gradually increase with the amount of miR-29b added into the buffer (Figure 2B). Particularly, in the presence of 250 nM of the analogue of miR-29b, around 70% of the immobilized FITC-labeled hpDNA strands are released from the Au@PDA NPs (Figure 2B, see inset), as estimated by comparing the recovered fluorescence signals in buffer with a standard curve acquired with known concentrations of the FITC-labeled hpDNA strands (Figure S8).⁴³

In addition to the release assay, we examine the specificity of the nanoprobes by using a random DNA sequence as control (sequence information listed in Table S1). 500 nM of the random sequence is added into the nanoprobes and incubated for 24 h. We observe negligible fluorescence signals from the

resultant solution (Figure S9). These data confirm that our nanoprobes can indeed release the quenched fluorescent hpDNAs immobilized onto the Au@PDA NPs upon the specific binding with the DNA analogue of the target miRNA in buffer, and prompt us to further investigate whether these nanoprobes can release fluorescent hpDNAs in the presence of specific miRNAs inside stem cells.

Cellular Uptake of Au@PDA NPs. We next investigate whether our nanoprobes can enter stem cells. Despite their negative surface charge of -39 mV (Table 1), we find that our as-synthesized Au@PDA NPs can naturally cross the cell membrane of hMSCs in abundant amounts without using any cationic²⁹ or lipophilic transfection agents⁴⁴ after 24 h of incubation. This is striking because stem cells, including hMSCs, are indeed difficult to transfect.¹⁶ After cellular entry, most Au@PDA NPs reside in the cytosol or lysosomes as individual particles or clusters, as evidenced by dark-field and TEM imaging data (Figure 3A, B). Moreover, most of the

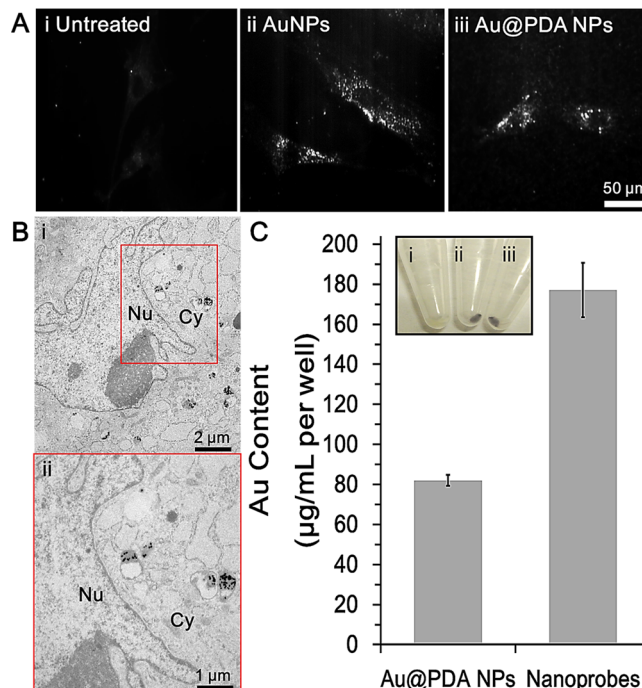


Figure 3. Evidence of cellular uptake by hMSCs. (A) Dark-field light-scattering images of (i) untreated hMSCs, (ii) AuNP-treated hMSCs, and (iii) Au@PDA NP-treated hMSCs. (B) (i) TEM micrographs of hMSCs incubated with Au@PDA NPs for 24 h. (ii) is the enlargement of boxed area of (i). Nu = nucleus, Cy = cytosol. (C) ICP-OES measurements of hMSCs treated with Au@PDA NPs and Au@PDA-hpDNA nanoprobes (nanoparticles) for 24 h. The Au content of cell-associated nanoparticles is determined by using a standard curve (Figure S12) and represented by Au content per well. Data obtained from 3 independent measurements are presented as mean \pm SD. Inset: Photographs of cell pellets collected for (i) untreated hMSCs, (ii) Au@PDA NP-treated hMSCs, and (iii) nanoprobe-treated hMSCs.

uptaken particles are located at the perinuclear region (Figure S10). Interestingly, ICP-OES data show that the adsorption of hpDNA strands onto the surface of Au@PDA NPs further increases the cellular uptake by \sim 2-fold (Figure 3C). These data reveal that both the PDA shell and the hpDNA oligonucleotides facilitate the uptake of AuNPs by hMSCs. After initial cellular uptake, we observe no obvious reduction in the intracellular Au content of cell-associated nanoparticles for

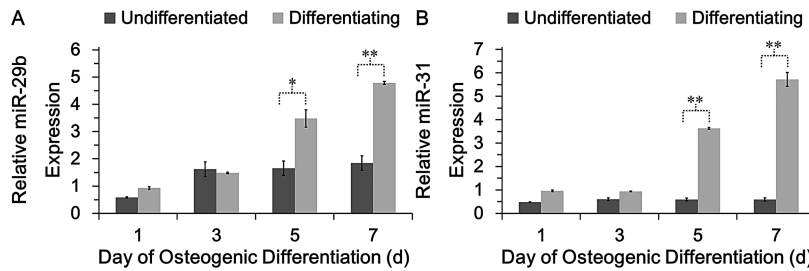


Figure 4. qRT-PCR measurements of two early osteogenic marker miRNAs (A) miR-29b and (B) miR-31 in hMSCs. The expression levels of both miR-29b and miR-31 are upregulated in the differentiating hMSCs under osteogenic induction. Statistically significant difference in the expression of miRNAs between the differentiating hMSCs and undifferentiated hMSCs is observed starting from Day 5. qRT-PCR is performed using small nuclear RNA gene U6 as the internal control. Data obtained from three independent measurements are presented as mean \pm SD * = $p < 0.05$; ** = $p < 0.005$.

hMSCs treated either with Au@PDA NPs or nanoprobes for up to 5 d of incubation, as revealed by our ICP-OES data (Figure S11B). These data suggest that both Au@PDA NPs and nanoprobes can stay inside the hMSCs for at least 5 days. Although the mechanism that governs the uptake of Au@PDA NPs by stem cells remains unclear at this point, Mirkin and co-workers have demonstrated that the attachment of DNA oligonucleotides onto the surface of AuNPs can support their cellular uptake.^{12,45} Furthermore, we speculate that the PDA coating may have contributed to the substantial cellular uptake of our nanoprobes.

Intracellular Detection of miRNAs in hMSCs and Monitoring of Differentiation Status. miR-29b is a well-known positive regulator of osteogenesis robustly expressed in osteoblastic cells.⁴⁶ Profiling studies show that the expression of miR-29b in preosteoblasts follows a temporal pattern in which the miR-29b level elevates with the time of osteoblast maturation.^{46,47} A similar trend of miR-29b expression can be observed in stem cells throughout the osteogenic differentiation.^{18,27} More recently, miR-31 has been found as another regulator of osteogenesis in hMSCs, which is significantly up-regulated in differentiating hMSCs.²⁶ Our in-house qRT-PCR results confirm a monotonically increasing trend in the cellular levels of both miR-29b and miR-31 in the differentiating hMSCs (upon osteogenic induction from Day 1 to Day 7) but not in the undifferentiated hMSCs (Figure 4). Moreover, it takes 5 d for the expression levels of these specific miRNAs in the differentiating hMSCs to be significantly more pronounced than those in the undifferentiated hMSCs. The dynamic intracellular levels of such specific miRNAs governed by the osteogenic differentiation inspire us to investigate whether the intracellular tracking of miR-29b and miR-31 can assist in the monitoring of the osteogenesis progress of stem cells or the identification of osteoblastic cells.

To test our hypothesis, ~0.025 nM of nanoprobes carrying immobilized FITC-labeled hpDNAs that specifically recognize miR-29b are incubated with hMSCs in basal medium (containing no osteogenesis-inducing factor). After 24 h of cellular uptake, hMSCs are thoroughly rinsed and cultured either in basal medium as control or in osteogenic induction medium⁵ in which hMSCs will progressively differentiate to osteoblasts. Confocal laser scanning microscopic (CLSM) images of the treated hMSCs are taken at different time points after uptake of the nanoprobes. Representative confocal images show weak but observable fluorescence signals (green channel) in the treated hMSCs after 1 d of osteogenic culture (Figure 5A), indicating that our nanoprobes are capable of detecting miRNA targets at a low initial concentration. The fluorescence

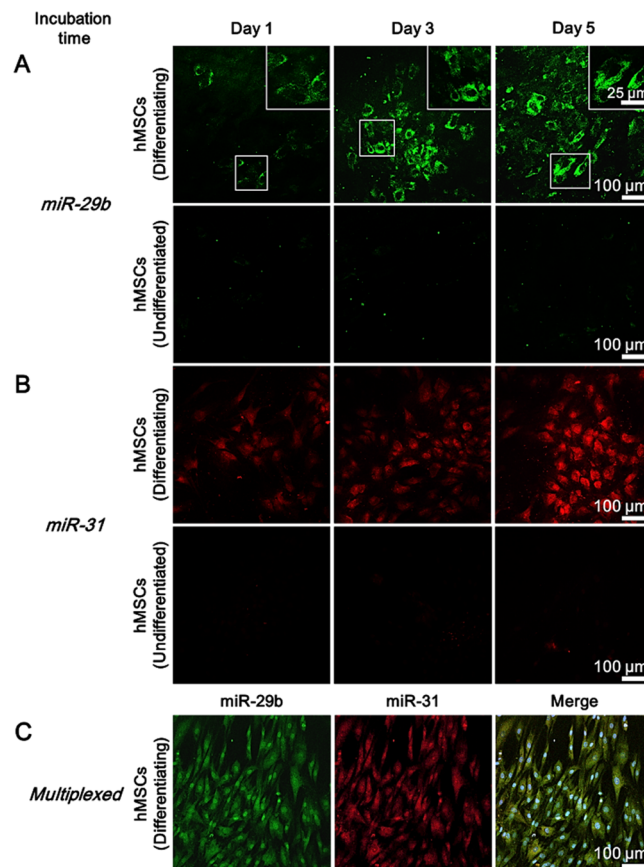


Figure 5. Monitoring of differentiation progress of hMSCs via the intracellular detection of miRNAs. (A) Confocal images of hMSCs treated with nanoprobes targeting miR-29b (green). Scale bar is 100 μ m. Inset: High-magnification images of the boxed area. Scale bar is 25 μ m. (B) Confocal images of hMSCs treated with nanoprobes targeting miR-31 (red). Scale bar is 100 μ m. Results show that hMSCs express detectable levels of miR-29b and miR-31 in a time-dependent manner and only when they undergo osteogenic differentiation. (C) Multiplexed detection of miR-29b and miR-31 in hMSCs upon 3 d of osteogenic induction. Results show that hMSCs express both the osteogenic marker miRNAs during osteogenesis. Nuclei are counterstained with Hoechst 33342. Scale bar is 100 μ m.

signals in the differentiating hMSCs increase significantly over time and become very intense on Day 5 (Figure 5A). These gradual and yet significant changes in intracellular fluorescence with osteoinduction time indeed match well with the increasing trend of miR-29b expression obtained in our qRT-PCR analysis

(Figure 4). High-magnification confocal images show significant fluorescence signals inside the differentiating hMSCs except for the nuclei (Figure 5A, see inset). Not all of the differentiating hMSCs exhibit the same level of fluorescence. This is probably due to the inherent variation in the differentiation potential among the hMSC population, which is known to be phenotypically heterogeneous.^{48,49} As a negative control experiment, the undifferentiated hMSCs cultured in basal medium do not show any significant FITC fluorescence over the same observation time window (Figure 5A). The sharp difference in fluorescence responses between the differentiating and undifferentiated hMSCs highlights the specificity and sensitivity of the Au@PDA-hpRNA nanoprobes in detecting miR-29b in living stem cells.

To demonstrate the versatility of our nanoprobes, we repeat the detection assay in hMSCs by using nanoprobes containing Cy3-labeled hpDNA strands to detect miR-31. Again, we observe increasing Cy3 fluorescence responses (red channel) over time only in the differentiating hMSCs but not the undifferentiated hMSCs (Figure 5B). For enhanced monitoring of the differentiation process, we have also prepared multiplexed Au@PDA–hpDNA nanoprobes for detecting both miR-29b and miR-31 in hMSCs. Successfully, we demonstrate that our nanoprobes can perform simultaneous detection of both specific miRNA targets in living hMSCs upon 3 d of osteogenic differentiation (Figure 5C).

In line with our previous results from qRT-PCR measurements, we observe a monotonic increase in fluorescence signals of the differentiating hMSCs for both the miR-29b and miR-31 detection as quantified by using ImageJ (Figure S13). The increment in cell fluorescence is indeed commensurate with an increase in the amount of intracellular miR-29b or miR-31. More importantly, a statistically significant difference in the level of miRNAs between the differentiating and undifferentiated hMSCs based on the qRT-PCR analysis can only be observed starting from 5 d of osteogenic induction, meaning that our nanoprobes appear to be more sensitive than the conventional qRT-PCR method for monitoring specific miRNA levels in living hMSCs at the early stage of osteogenic differentiation.

For both the FITC and Cy3 probes, the target-triggered fluorescence signals from the nanoprobes persist inside the differentiating hMSCs up to 5 d after initial cellular entry. Taken together, the results underscore the stability of the nanoprobes and their capability of monitoring the differentiation progress of hMSCs. To the best of our knowledge, this is the first study that reports the long-term tracking of miRNA expression inside living stem cells.

Performance Evaluation of Intracellular miRNA Detection.

To evaluate the unique properties of our Au@PDA–hpDNA nanoprobes for intracellular miRNA detection, we next compare the performance of our nanoprobes with that of SmartFlare, the commercialized version of the NanoFlare, as an intracellular RNA detection probe. We choose miR-29b as the target marker miRNA for comparing both detection systems. We employ Cy3-labeled SmartFlare against miR-29b for the comparative studies in order to distinguish its fluorescence signals from our FITC-labeled nanoprobes against miR-29b. By strictly following the manufacturer's protocol, we first seek to detect miR-29b in hMSCs in a “continuous administration” manner. That is, we replenish hMSCs with fresh SmartFlare 24 h before each designated observation time point (i.e., Day 0, Day 2, and Day 4). Upon osteogenic

induction, we observe a time-dependent increase in Cy3 fluorescence signals (red channel) in the differentiating hMSCs, whereas the undifferentiated hMSCs only show weak fluorescence (Figure 6A). These results coincide with the

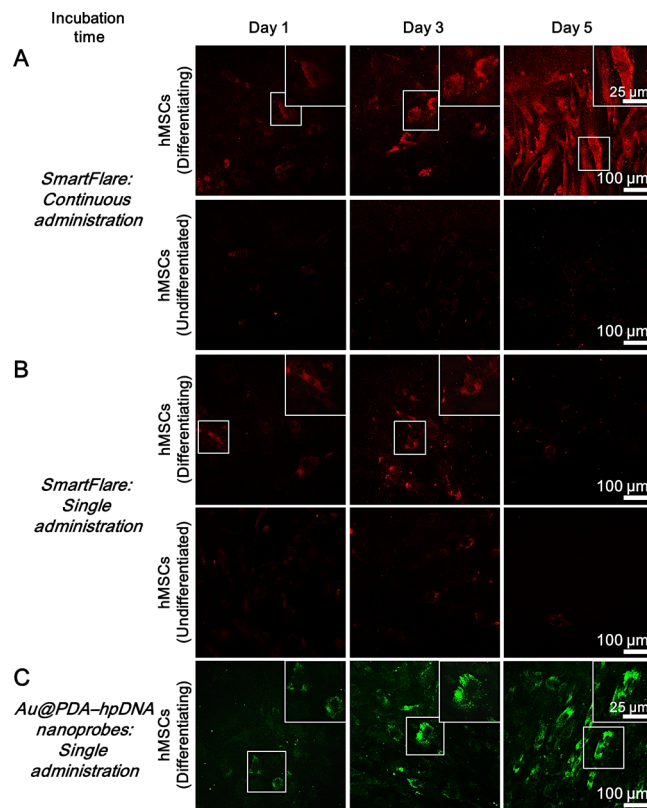


Figure 6. Comparison of our Au@PDA–hpDNA nanoprobes with the commercially available RNA detection probe SmartFlare. (A) Intracellular detection of miR-29b in hMSCs using Cy3-labeled SmartFlare against miR-29b with a continuous administration. We observe an increasing Cy3 fluorescence signals from SmartFlare only in the differentiating hMSCs but not the undifferentiated hMSCs. Scale bar is 100 μm . (B) Intracellular detection of miR-29b in hMSCs using Cy3-labeled SmartFlare against miR-29b with a single administration. We observe that fluorescence responses from SmartFlare disappear in the differentiating hMSCs after 5 d of culture. Scale bar is 100 μm . (C) Intracellular detection of miR-29b in hMSCs using a single administration of our FITC-labeled Au@PDA–hpDNA nanoprobes against miR-29b. We observe stable fluorescence signals in the differentiating hMSCs even after 5 d of culture. Scale bar is 100 μm . Insets: High-magnification images of the boxed area. Scale bar is 25 μm .

previous observations based on our Au@PDA–hpDNA nanoprobes, reinforcing our claim that our nanoprobes are capable of monitoring the dynamic expression of miR-29b in differentiating hMSCs.

It is worth noting that our nanoprobes require only a single administration to hMSCs on the initial day of study and that fluorescence signals observed in the differentiating hMSCs can persist up to 5 days. Therefore, we next investigate whether SmartFlare can also perform long-term tracking of miR-29b in living stem cells. To do so, we introduce SmartFlare to hMSCs only once and then observe the fluorescence responses over the same observation time window without replenishing the cells with fresh SmartFlare. Without continuous administration, we observe in at least three independent experiments that

fluorescence responses from SmartFlare in the differentiating hMSCs start to disappear after 3 d of osteogenic induction (Figure 6B). Indeed, the fluorescence responses of SmartFlare are noticeably weaker than those of our Au@PDA–hpDNA nanoprobes. After 5 d of osteogenic induction, the intracellular fluorescence signals displayed by SmartFlare have virtually vanished, whereas those exhibited by our nanoprobes are still very stable (Figure 6C). These data indicate that our nanoprobes possess a significantly longer intracellular observation time window than that of SmartFlare. Even though we observe no strong fluorescence signal in hMSCs on Day 7 of osteogenic induction (data not shown), we have demonstrated that our Au@PDA–hpDNA nanoprobes outperform other commercial RNA detection probes such as SmartFlare in terms of the capability of long-term tracking of miRNAs in living stem cells.

We speculate that efficient cellular entry in hMSCs may have contributed to the superior ability of our Au@PDA–hpDNA nanoprobes for long-term intracellular tracking. To address this, we treat hMSCs with either our nanoprobes or SmartFlare at an identical concentration (i.e., 0.025 nM) for 24 h, and subsequently utilize ICP-OES to quantify the intracellular Au content. Strikingly, uptake of our nanoprobes by hMSCs is ~7-fold higher than that of SmartFlare (Figure S14B). This reveals more favorable cellular uptake by hMSCs, possibly attributed by the size difference in the nanoparticles^{36,37} and the presence of the PDA shell. By literature precedent, adsorption of DNA strands onto the surface of PDA nanospheres results in protection of the DNA against enzymatic degradation.⁵⁰ We hypothesize that enhanced nuclease resistance of our nanoprobes, provided by the PDA shell, also contributes to their high stability in intracellular environment.

Intracellular Detection of miRNAs in Primary Osteoblasts and 3T3 Fibroblasts. To further evaluate the ability of Au@PDA–hpDNA nanoprobes to detect miRNAs in other cell types, we repeat the same procedures for detecting miR-29b by using primary osteoblasts and 3T3 fibroblasts. Osteoblasts, which constitutively express high levels of miR-29b during growth,^{42,43} are used here as the positive control for hMSCs undergoing osteogenic differentiation. Meanwhile, 3T3 fibroblasts, which express the minimal level of miR-29b,⁵¹ are chosen as the negative control. Osteoblasts and 3T3 fibroblasts are treated identically as hMSCs with the nanoprobes against miR-29b before confocal imaging. As expected, the osteoblasts exhibit the highest level of fluorescence signals among the three tested cell types after 5 d of culture (Figure 7A). Interestingly, we observe a nearly constant level of fluorescence in the osteoblasts from Day 1 to Day 5 of culture. In sharp contrast, 3T3 fibroblasts show negligible fluorescence signals after the same period of culture (Figure 7B).

To confirm that the bright fluorescence signals observed in the differentiating hMSCs and the living osteoblasts do not stem from the intracellular degradation by nucleases, Au@PDA–hpDNA nanoprobes carrying a FITC-labeled scrambled DNA sequence (sequence information listed in Table S1) are incubated with the same cell types as a negative control study. Confocal images show no obvious fluorescence response in both osteoblasts and differentiating hMSCs even after 5 d of culture (Figure S15). Taken together, these results demonstrate that the Au@PDA–hpDNA nanoprobes are capable of elucidating the relative expression of specific miRNA target(s) in various types of mammalian cells.

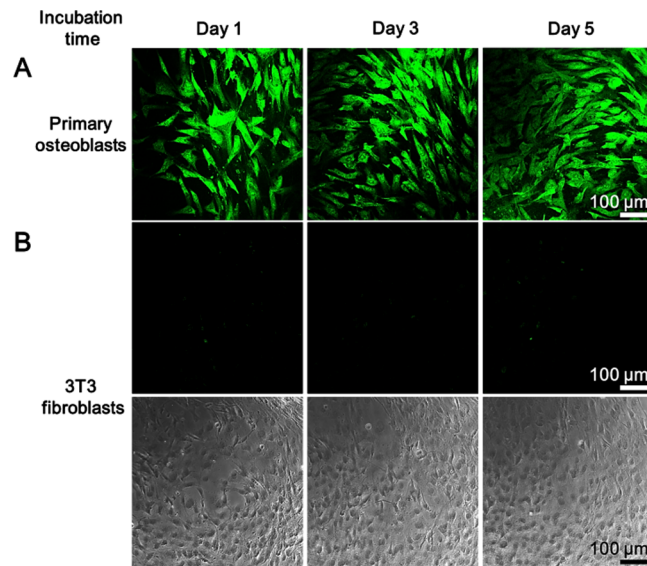


Figure 7. Intracellular detection of miR-29b in (A) primary osteoblasts and (B) 3T3 fibroblasts. Representative confocal images show that osteoblasts highly express miR-29b whereas 3T3 fibroblasts do not. Corresponding bright-field images of 3T3 fibroblasts are shown in the bottom panel for reference. Scale bar is 100 μ m.

CONCLUSIONS

We report in this work the sequence-specific detection of two osteogenic marker miRNAs, namely, miR-29b and miR-31, in living stem cells by using our cell-penetrating Au@PDA–hpDNA nanoprobes. We have demonstrated that our nanoprobes outperform the conventional methods (e.g., qRT-PCR analysis and staining) and the existing commercial intracellular RNA detection probe (e.g., SmartFlare) in the context of long-term intracellular detection of miRNAs (see Table S3). More significantly, we have not only established an approach to distinguishing differentiating stem cells from undifferentiated stem cells, but also demonstrated the time-dependent and dynamic expression of specific miRNAs in differentiating stem cells. The capability of our nanoprobes for the multiplexed detection of miRNAs allows for enhanced monitoring of cellular events (e.g., differentiation) in living stem cells. In addition, the specificity of our nanoprobes enables the identification of osteoblastic cells such as primary osteoblasts from nonosteoblastic cells such as 3T3 fibroblasts. More importantly, our nanoprobes afford long-term tracking of intracellular miRNAs in living stem cells, which cannot be achieved by commercially available RNA detection probe such as SmartFlare. The modular design of our nanoprobes offers facile switching of customized hairpin DNA probes (including the type of fluorescent labels and sequence), thus opening up an avenue for detecting other biomarkers such as mRNAs in living stem cells. We believe that our Au@PDA–hpDNA nanoprobes hold great promise in the investigation of the dynamics of stem cell differentiation, the identification and isolation of specific cell types, and high-throughput drug screening.

EXPERIMENTAL SECTION

Synthesis of AuNP@PDA NPs. All chemicals used in this study were ordered from Sigma Adrich unless otherwise specified. Citrate-capped AuNPs of ~40 nm in diameter were synthesized in accordance with a previously reported method,³³ but with minor modifications.

The concentration of AuNPs was determined by an Optima 4300DV inductively coupled plasma optical emission spectrometer (PerkinElmer). Freshly prepared AuNPs were coated with a PDA shell. To decorate the gold core with a PDA shell of ~5 nm in thickness, 10 mL of the AuNP stock solution (~0.1 nM) was mixed with 10 mL of the dopamine solution (0.1 mg/mL, buffered in 10 mM Tris at pH 8.5) under continuous sonication at 20 kHz (Banson) for 1 h at room temperature. Purification of the as-prepared Au@PDA NPs was achieved by repeated centrifugation (Hettich) at 13 500 rpm for 10 min. The purified Au@PDA NPs were redispersed in Nanopure water (Thermo Scientific).

Characterization of Au@PDA NPs. The UV-vis absorption spectra of the AuNP and Au@PDA NP solutions were recorded with a Cary 5000 UV-vis spectrophotometer (Agilent). The functional groups of AuNPs before and after PDA coating were analyzed with a Nicolet iS10 Fourier transform infrared spectrometer (Thermo Scientific). The nanoparticles were imaged by a Techni TS12 electron microscope (FEI) by using a beam voltage of 120 kV. Over 100 particles were selected in multiple images from different areas of the copper grid (Electron Microscopy Sciences) and measured to determine the physical size by using ImageJ (NIH). Hydrodynamic size and zeta potential were determined by a ZetaPlus zeta potential analyzer (Brookhaven Instruments).

Synthesis of Au@PDA-hpDNA Nanoprobes. All oligonucleotides used for this study were purchased (TaKaRa) and used without further purification. In a typical synthesis, Au@PDA-hpDNA nanoprobes (including nanoprobes that contain a scrambled DNA sequence) were prepared via the immobilization of fluorescently labeled hpDNAs on the surface of Au@PDA NPs. To achieve this, 2 mL of ~0.1 nM of Au@PDA NP solution was concentrated 10 times by centrifugation. 200 μ L of 500 nM the DNA solution (prepared in PBS) was then added to disperse the pellet and the mixture was allowed to incubate at room temperature for 1 h. Excess DNA strands were removed by centrifugation (Eppendorf). The pellet was redispersed in water to restore the initial concentration of the AuNP stock. For the multiplexed nanoprobes, 100 μ L of FITC-labeled hpDNAs against miR-29b (500 nM) and 100 μ L of Cy3-labeled hpDNAs against miR-31 (500 nM) were mixed first before incubating with Au@PDA NPs.

Quenching and Release Assay of Nanoprobes. To monitor the immobilization of hpDNA probes onto the surface of Au@PDA NPs, fluorescence measurements were carried out by using a fluorescence spectrophotometer (Hitachi). The experimental procedures are graphically illustrated in Scheme S1. Briefly, the mixture of hpDNAs and Au@PDA NPs after 1 h of incubation was spun down and the supernatant was extracted for further investigation. The fluorescence signal of the free hpDNA solution was recorded as the reference. The DNA analogue of miR-29b (i.e., the complementary DNA sequence of the recognition region of the hpDNA probe against miR-29b) was used as the target for the extracellular studies. Subsequently, the nanoprobes carrying immobilized FITC-labeled hpDNA-29b (100 nM) were mixed with different concentrations of target (0, 10, 25, 50, 125, 250, and 500 nM) and allowed to hybridize for 2 h. The mixture was then centrifuged and the supernatant was extracted to obtain the release profile. The recorded fluorescence intensity was compared with the reference intensity. A random DNA sequence was used to test the specificity of the nanoprobes against miR-29b in buffer.

Cell Culture. All cell experiments associated were conducted at 37 °C and 5% CO₂. hMSCs (Lonza) were expanded to Passage 3 in basal medium (α -MEM supplemented with 10% FBS, 1% streptomycin/penicillin, and 1% L-glutamine; Invitrogen). To induce osteogenesis, hMSCs were cultured in induction medium (basal medium added with 10 mM bone morphogenetic protein, 50 μ g/mL L-ascorbic acid 2-phosphate, and 100 nM dexamethasone). Primary mouse osteoblasts were a gift from Professor Gang Li of The Chinese University of Hong Kong. Osteoblasts were grown and expanded to Passage 3 in DMEM supplied with 10% FBS, 1% streptomycin/penicillin, and 1% L-glycine. 3T3 mouse fibroblasts were expanded in basal medium.

Cell Viability. hMSCs were seeded at a density of 5000 cells/cm² and grown to 80–90% confluence. Cells were then incubated with nanoparticles at varying concentrations (0.01–0.05 nM) for 24 h. The viability of the cells was estimated by the Alamar blue assay (Invitrogen). All experiments were carried out in triplicate. The nanoparticle-associated cytotoxicity was represented as the absorbance at 570 nm normalized by the data from untreated hMSCs.

Dark-Field Microscopy. The cellular uptake of the nanoparticles by hMSCs was qualitatively examined by dark-field microscopy, using an inverted IX70 microscope equipped with an illumination condenser (Olympus). Cells were grown on 35 mm coverglass bottom dish (SPL Lifescience) and treated with ~0.025 nM of nanoparticles (both AuNPs and Au@PDA NPs) for 24 h. Cells were thoroughly rinsed with DPBS (Invitrogen) before imaging.

TEM. hMSCs were grown in a 6-well plate (SPL Lifescience) to 80–90% confluence and incubated with ~0.025 nM of Au@PDA NPs for 24 h. The treated cells were then trypsinized and centrifuged. The cell pellets were fixed in 4% paraformaldehyde (PFA) in PBS for 15 min. Cells were then centrifuged again and the pellets were enrobed in molten 2% agarose at 37 °C. The mixture was then gelated in water at room temperature. Afterward, the cell-containing gels were fixed in 2.5% glutaraldehyde in 100 mM sodium cacodylate buffer (pH = 7.4), stained by 1% OsO₄ and by 0.9% OsO₄ and 0.3% K₄Fe(CN)₆, with all steps carried out at 4 °C for 2 h. The treated gels were gradually dehydrated with ethanol and propylene oxide. Following that, the cell-containing gels were embedded in Epon 812 resins (Electron Microscopy Sciences) and further polymerized. The sectioned samples (80 nm) were finally deposited on 200-mesh copper grids (Electron Microscopy Sciences) and stained with 2% uranyl acetate (SPI Supplies) and Reynolds lead citrate. The TEM images were recorded under a H7700 Transmission Electron Microscope (Hitachi), using a beam voltage of 80 kV.

ICP-OES. hMSCs were grown in a 24-well plate (SPL Lifescience) to 80–90% confluence and incubated with ~0.025 nM of nanoparticles for 24 h. Following that, the treated cells were thoroughly rinsed. Cell pellets were obtained and then digested in 0.25 mL of freshly prepared aqua regia (HCl:HNO₃ = 1:3, v/v) at 55 °C for 30 min. After adding 0.08 mL of 1000 ppm indium (internal standard; AccuStandard) and 3.52 mL of matrix solution (2% HCl and 2% HNO₃), the atomic Au content in the resultant solution was determined by ICP-OES. The data obtained from untreated hMSCs were used for background correction.

qRT-PCR Measurements of miRNAs. Relative expression of mature hsa-miR-29b-3p and hsa-miR-31 was evaluated by using the QuantiMir RT kit (System Biosciences) followed by qRT-PCR analysis according to the manufacturer's instruction, but with minor modifications. Briefly, the microRNAs were tagged with poly A tail, annealed with an oligo-dT adaptor, and converted into first strand cDNA. qRT-PCR was then performed with the following primers by using the KAPA SYBR FAST qPCR kit (Kapa Biosystems) in a LightCycler 480 Instrument I (Roche Applied Science): miR-29b-3p forward, 5'-TAG CAC CAT TTG AAA TCA GTG TT-3'; miR-31 forward, 5'-AGG CAA GAT GCT GGC ATA GCT-3'; U6 forward, 5'-CTC GCT TCG GCA GCA CA-3', and a universal reverse primer supplied in the assay kit. The analysis was performed at 95 °C for 5 min, followed by 50 cycles of 95 °C for 10 s and 60 °C for 10 s. Fluorescence signal was acquired at the end of the elongation step of every PCR cycle to monitor the increasing amount of amplified DNA. ΔCt was first calculated by subtracting the Ct of U6 from that of the measured microRNA. $\Delta\Delta Ct$ was then calculated by subtracting the ΔCt of the undifferentiated hMSCs from the ΔCt of the differentiated hMSCs. Following that, fold change of microRNA expression was then calculated by the eq $2^{-\Delta\Delta Ct}$. All the measurements were conducted in triplicates. Melting curve analysis was performed after the amplification phase to eliminate the possibility of nonspecific amplification or primer dimer formation.

Confocal Microscopy. For all of the tested cell types, cells were seeded on coverglass bottom dish and allowed to grow to 80–90% confluence. Following that, cells (remained in their undifferentiated state) were treated with ~0.025 nM of nanoprobes dispersed in basal

medium for 24 h. Then, the medium containing nanoprobes was aspirated and the cells were washed with DPBS (Invitrogen) thrice. Fresh medium was added and the cells were allowed to either grow or differentiate (for hMSCs). At each selected time point (i.e., 1, 3, and 5 d after incubation), cells were imaged under a TCS SP8 confocal scanning microscope (Leica). The excitation wavelengths for FITC and Cy3 are 488 and 514 nm, respectively. To avoid misinterpretation of the fluorescence responses from cells, imaging conditions were kept constant for all the samples with the same fluorescence dye involved. Images were analyzed by ImageJ (NIH). Over 50 cells per sample were chosen for the quantification of cell fluorescence.

Long-Term Evaluation. SmartFlare (EMD Millipore) against hsa-miR-29b-3p was employed for the comparative study and used according to the manufacturer's instructions. Briefly, the lyophilized particles were reconstituted as a 100 nM stock in 50 μ L of ultrapure water (Invitrogen). Before adding to the cell culture, the stock solution was diluted 20 times in PBS. Twenty μ L of the working solution were added into hMSCs grown in 1 mL of basal medium. Cells were incubated with the probes for 24 h and washed with DPBS thrice. Additional administration was carried out in the same manner 24 h before the day of confocal imaging.

Statistical Analysis. Unless otherwise mentioned, all data are presented as mean \pm standard deviation. Statistical analysis was performed using Student's *t*-test. *P*-values of <0.05 and <0.005 were considered to be statistically significant and highly significant, respectively.

■ ASSOCIATED CONTENT

Supporting Information

Oligonucleotide sequences involved in this work, properties of nanoprobes, primer sequence employed for the qRT-PCR of gene expression, qRT-PCR results, staining results, data of DLS measurements, additional TEM images of Au@PDA NPs, FT-IR spectra, stability test of Au@PDA NPs, cytotoxicity assay, standard curve of fluorescently labeled hpDNAs, release and specificity assays of nanoprobes, additional TME images of hMSCs treated with Au@PDA NPs, additional ICP-OES data, standard curve of gold standard solutions, quantification of cell fluorescence, intracellular specificity and stability assays of nanoprobes, and scheme of preparation of nanoprobes. The Supporting Information is available free of charge on the ACS Publications website at DOI: 10.1021/jacs.5b01457.

■ AUTHOR INFORMATION

Corresponding Authors

*jchchoi@ee.cuhk.edu.hk
*lbian@mae.cuhk.edu.hk

Notes

The authors declare no competing financial interest.

■ ACKNOWLEDGMENTS

The work described in this paper was supported by an Early Career Scheme grant from the Research Grants Council of Hong Kong (Project No. 439913). This research was supported by project BME-8115043 of the Shun Hing Institute of Advanced Engineering, The Chinese University of Hong Kong (CUHK). This research was supported by Chow Yuk Ho Technology Centre for Innovative Medicine, CUHK. This research was supported by an Innovation Technology Fund (ITF, Tier 3, ITS/218/13), Hong Kong. The authors would like to thank Dr. Wayne Lee and Professor Gang Li from the Department of Orthopaedics and Traumatology (CUHK) for their generous contribution of mouse primary osteoblasts and related supplies. The authors would also like to thank Mr. Kin Pan Chung and Professor Liwen Jiang from the Department of

Biology (CUHK) for their help in conducting the confocal microscopy experiments. Dark-field microscopy and TEM imaging were performed at the Department of Physics (CUHK). FT-IR spectroscopy, ICP-OES, and DLS measurements were performed at the Department of Chemistry (CUHK). Confocal microscopy was performed in the Centre for Cell and Developmental Biology (CUHK). Ultramicrotomy and bio-TEM imaging were performed in the School of Biomedical Sciences (CUHK).

■ REFERENCES

- (1) Pittenger, M. F.; Mackay, A. M.; Beck, S. C.; Jaiswal, R. K.; Douglas, R.; Mosca, J. D.; Moorman, M. A.; Simonetti, D. W.; Craig, S.; Marshak, D. R. *Science* **1999**, *284*, 143.
- (2) Abdallah, B. M.; Kassem, M. *Gene Ther.* **2008**, *15*, 109.
- (3) Caplan, A. I. *J. Cell. Physiol.* **2007**, *213*, 341.
- (4) Granchi, D.; Ochoa, G.; Leonardi, E.; Devescovi, V.; Baglio, S. R.; Osaba, L.; Baldini, N.; Ciapetti, G. *Tissue Eng., Part C* **2010**, *16*, 511.
- (5) Grigoriadis, A. E.; Heersche, J. N.; Aubin, J. E. *J. Cell Biol.* **1988**, *106*, 2139.
- (6) Fukuda, H.; Takahashi, J.; Watanabe, K.; Hayashi, H.; Morizane, A.; Koyanagi, M.; Sasai, Y.; Hashimoto, N. *Stem Cells* **2006**, *24*, 763.
- (7) Pruszak, J.; Sonntag, K. C.; Aung, M. H.; Sanchez-Pernaute, R.; Isacson, O. *Stem Cells* **2007**, *25*, 2257.
- (8) Kim, T. H.; Lee, K. B.; Choi, J. W. *Biomaterials* **2013**, *34*, 8660.
- (9) Seferos, D. S.; Giljohann, D. A.; Hill, H. D.; Prigodich, A. E.; Mirkin, C. A. *J. Am. Chem. Soc.* **2007**, *129*, 15477.
- (10) Prigodich, A. E.; Randeria, P. S.; Briley, W. E.; Kim, N. J.; Daniel, W. L.; Giljohann, D. A.; Mirkin, C. A. *Anal. Chem.* **2012**, *84*, 2062.
- (11) Halo, T. L.; McMahon, K. M.; Angeloni, N. L.; Xu, Y.; Wang, W.; Chinen, A. B.; Malin, D.; Strekalova, E.; Cryns, V. L.; Cheng, C.; Mirkin, C. A.; Thaxton, C. S. *Proc. Natl. Acad. Sci. U. S. A.* **2014**, *111*, 17104.
- (12) Choi, C. H. J.; Hao, L.; Narayan, S. P.; Auyeung, E.; Mirkin, C. A. *Proc. Natl. Acad. Sci. U. S. A.* **2013**, *110*, 7625.
- (13) Prigodich, A. E.; Alhasan, A. H.; Mirkin, C. A. *J. Am. Chem. Soc.* **2011**, *133*, 2120.
- (14) Cutler, J. I.; Auyeung, E.; Mirkin, C. A. *J. Am. Chem. Soc.* **2012**, *134*, 1376.
- (15) Tyagi, S. *Nat. Methods* **2009**, *6*, 331.
- (16) Eguchi, A.; Meade, B. R.; Chang, Y. C.; Fredrickson, C. T.; Willert, K.; Puri, N.; Dowdy, S. F. *Nat. Biotechnol.* **2009**, *27*, 567.
- (17) Wu, X. A.; Choi, C. H. J.; Zhang, C.; Hao, L.; Mirkin, C. A. *J. Am. Chem. Soc.* **2014**, *136*, 7726.
- (18) Stefani, G.; Slack, F. J. *Nat. Rev. Mol. Cell Biol.* **2008**, *9*, 219.
- (19) Hobert, O. *Science* **2008**, *319*, 1785.
- (20) Huntzinger, E.; Izaurralde, E. *Nat. Rev. Genet.* **2011**, *12*, 99.
- (21) Chen, C. Z.; Li, L.; Lodish, H. F.; Bartel, D. P. *Science* **2004**, *303*, 83.
- (22) Mizuno, Y.; Yagi, K.; Tokuzawa, Y.; Kanesaki-Yatsuka, Y.; Suda, T.; Katagiri, T.; Fukuda, T.; Maruyama, M.; Okuda, A.; Amemiya, T.; Kondoh, Y.; Tashiro, H.; Okazaki, Y. *Biochem. Biophys. Res. Commun.* **2008**, *368*, 267.
- (23) Ivey, K. N.; Muth, A.; Arnold, J.; King, F. W.; Yeh, R. F.; Fish, J. E.; Hsiao, E. C.; Schwartz, R. J.; Conklin, B. R.; Bernstein, H. S.; Srivastava, D. *Cell Stem Cell* **2008**, *2*, 219.
- (24) Suh, M. R.; Lee, Y.; Kim, J. Y.; Kim, S. K.; Moon, S. H.; Lee, J. Y.; Cha, K. Y.; Chung, H. M.; Yoon, H. S.; Moon, S. Y.; Kim, V. N.; Kim, K. S. *Dev. Biol.* **2004**, *270*, 488.
- (25) Suh, J. S.; Lee, J. Y.; Choi, Y. S.; Chung, C. P.; Park, Y. J. *Biomaterials* **2013**, *34*, 4347.
- (26) Baglio, S. R.; Devescovi, V.; Granchi, D.; Baldini, N. *Gene* **2013**, *527*, 321.
- (27) Kaneto, C. M.; Lima, P. S.; Zanette, D. L.; Prata, K. L.; Pina Neto, J. M.; de Paula, F. J.; Silva, W. A., Jr. *BMC Med. Genet.* **2014**, *15*, 45.

- (28) Lin, L. S.; Cong, Z. X.; Cao, J. B.; Ke, K. M.; Peng, Q. L.; Gao, J.; Yang, H. H.; Liu, G.; Chen, X. *ACS Nano* **2014**, *8*, 3876.
- (29) Dong, H.; Ding, L.; Yan, F.; Ji, H.; Ju, H. *Biomaterials* **2011**, *32*, 3875.
- (30) Ryoo, S. R.; Lee, J.; Yeo, J.; Na, H. K.; Kim, Y. K.; Jang, H.; Lee, J. H.; Han, S. W.; Lee, Y.; Kim, V. N.; Min, D. H. *ACS Nano* **2013**, *7*, 5882.
- (31) Dubertret, B.; Calame, M.; Libchaber, A. J. *Nat. Biotechnol.* **2001**, *19*, 365.
- (32) Qiang, W.; Li, W.; Li, X.; Chen, X.; Xu, D. *Chem. Sci.* **2014**, *5*, 3018.
- (33) Bastus, N. G.; Comenge, J.; Puntes, V. *Langmuir* **2011**, *27*, 11098.
- (34) Lee, H.; Dellatore, S. M.; Miller, W. M.; Messersmith, P. B. *Science* **2007**, *318*, 426.
- (35) Black, K. C.; Yi, J.; Rivera, J. G.; Zelasko-Leon, D. C.; Messersmith, P. B. *Nanomedicine* **2013**, *8*, 17.
- (36) Chithrani, B. D.; Ghazani, A. A.; Chan, W. C. *Nano Lett.* **2006**, *6*, 662.
- (37) Jiang, W.; Kim, B. Y.; Rutka, J. T.; Chan, W. C. *Nat. Nanotechnol.* **2008**, *3*, 145.
- (38) Jiang, J.; Zhu, L.; Zhu, L.; Zhu, B.; Xu, Y. *Langmuir* **2011**, *27*, 14180.
- (39) Liu, X.; Cao, J.; Li, H.; Li, J.; Jin, Q.; Ren, K.; Ji, J. *ACS Nano* **2013**, *7*, 9384.
- (40) Ham, H. O.; Liu, Z.; Lau, K. H.; Lee, H.; Messersmith, P. B. *Angew. Chem., Int. Ed.* **2011**, *50*, 732.
- (41) Liu, Q.; Pu, Z.; Asiri, A. M.; Al-Youbi, A. O.; Sun, X. *Sens. Actuators, B* **2014**, *191*, 567.
- (42) Yang, R.; Jin, J.; Chen, Y.; Shao, N.; Kang, H.; Xiao, Z.; Tang, Z.; Wu, Y.; Zhu, Z.; Tan, W. *J. Am. Chem. Soc.* **2008**, *130*, 8351.
- (43) Demers, L. M.; Mirkin, C. A.; Mucic, R. C.; Reynolds, R. A., 3rd; Letsinger, R. L.; Elghanian, R.; Viswanadham, G. *Anal. Chem.* **2000**, *72*, 5535.
- (44) Huang, L.; Li, S. *Nat. Biotechnol.* **1997**, *15*, 620.
- (45) Giljohann, D. A.; Seferos, D. S.; Patel, P. C.; Millstone, J. E.; Rosi, N. L.; Mirkin, C. A. *Nano Lett.* **2007**, *7*, 3818.
- (46) Li, Z.; Hassan, M. Q.; Jafferji, M.; Aqeilan, R. I.; Garzon, R.; Croce, C. M.; van Wijnen, A. J.; Stein, J. L.; Stein, G. S.; Lian, J. B. *J. Biol. Chem.* **2009**, *284*, 15676.
- (47) Kapinas, K.; Kessler, C.; Ricks, T.; Gronowicz, G.; Delany, A. M. *J. Biol. Chem.* **2010**, *285*, 25221.
- (48) Sekiya, I.; Larson, B. L.; Smith, J. R.; Pochampally, R.; Cui, J. G.; Prockop, D. J. *J. Stem Cells* **2002**, *20*, 530.
- (49) Bruder, S. P.; Jaiswal, N.; Haynesworth, S. E. *J. Cell. Biochem.* **1997**, *64*, 278.
- (50) Xie, Y.; Lin, X.; Huang, Y.; Pan, R.; Zhu, Z.; Zhou, L.; Yang, C. J. *Chem. Commun.* **2015**, *51*, 2156.
- (51) Jiao, J.; Herl, L. D.; Farese, R. V.; Gao, F. B. *PLoS One* **2010**, *5*, e10551.